Field-Induced Orbital Antiferromagnetism in Mott Insulators

K. A. Al-Hassanieh,[1] C. D. Batista,[1] G. Ortiz,[2] and L. N. Bulaevskii[1]

[1]*Theoretical Division, Los Alamos National Laboratory, Los Alamos, New Mexico 87545, USA*

[2]*Department of Physics, Indiana University, Bloomington, Indiana 47405, USA*

(Received 28 May 2009; published 19 November 2009)

We report on a new electromagnetic phenomenon that emerges in Mott insulators. The phenomenon manifests as antiferromagnetic ordering due to orbital electric currents which are spontaneously generated from the coupling between spin currents and an external homogenous magnetic field. This novel spin-charge-current effect provides the mechanism to measure the so-far elusive spin currents by means of unpolarized neutron scattering, nuclear magnetic resonance or muon spectroscopy. We illustrate this mechanism by solving a half-filled Hubbard model on a frustrated ladder.

DOI: 10.1103/PhysRevLett.103.216402 PACS numbers: 71.10.Fd, 72.80.Sk, 73.22.Gk, 74.25.Ha

Mott insulators are driven by intra-atomic electron-electron Coulomb interactions, and the half-filled (one electron per site) Hubbard Hamiltonian is the minimal model that describes its properties. While electrons are completely localized in the Wannier orbitals of band insulators, Mott insulators always exhibit a partial electronic delocalization due to the finitude of the Coulomb repulsion, U, relative to the kinetic energy. The combination of partial delocalization with the Pauli principle leads to the well known antiferromagnetic exchange, J, between localized spins $\mathbf{S}_j$. While this exchange coupling is responsible for the usual magnetic ordering, $\langle \mathbf{S}_j \rangle \neq 0$, the combination of geometric frustration and low space dimensionality may lead to more exotic thermodynamic phases. The vector and scalar chiralities

$$\boldsymbol{\kappa}_{jk} = \mathbf{S}_j \times \mathbf{S}_k, \qquad \chi_{jkl} = \mathbf{S}_j \times \mathbf{S}_k \cdot \mathbf{S}_l, \tag{1}$$

are examples of observables that lead to exotic order parameters $\langle \boldsymbol{\kappa}_{jk} \rangle \neq 0$ or $\langle \chi_{jkl} \rangle \neq 0$, in absence of usual magnetic ordering ($\langle \mathbf{S}_j \rangle = 0$).

Vector chiral ordering, $\langle \boldsymbol{\kappa}_{jk} \rangle \neq 0$, was reported several years ago in frustrated quantum spin ladders [1]. As noted in [2], the weakly coupled ladders should exhibit a window of finite temperatures in which the vector chiral ordering exists in absence of usual magnetic ordering. The reason is that the chiral correlation length is much longer than the spin correlation length. There are experimental indications of the existence of such a phase in the quasi-one-dimensional organic magnet $Gd(hfac)_3NITiPr$ [3–5]. However, the absence of external physical fields that couple directly to $\boldsymbol{\kappa}_{jk}$ poses a challenge for measuring this chiral order parameter [6]. A main purpose of this Letter is to provide a physical mechanism to detect this exotic phase by means of unpolarized neutron scattering (NS), nuclear magnetic resonance (NMR), or muon spectroscopy (μSR). We achieve this goal by showing that an applied magnetic field along the z axis induces a nonzero scalar chirality that is proportional to the vector chiral order parameter $\langle \chi_{jj+1j+2} \rangle \propto \langle \kappa^z_{jj+1} \rangle$. As shown in Ref. [7], a nonzero scalar spin chirality leads to orbital electric currents in frustrated geometries. Based on this result, we will show here that the induced scalar chirality can be easily measured because it is slaved to a staggered ordering of orbital magnetic moments, i.e., to *orbital antiferromagnetism*.

Consider a Hubbard Hamiltonian on an L-site ($0 \leq j \leq L-1$) zigzag ladder (see Fig. 1), with nearest- (next-nearest-) neighbor hopping amplitudes t_1 (t_2), in an applied magnetic field $\mathbf{B} = B\hat{\mathbf{z}}$,

$$H = \sum_{j,\nu,\sigma} (t_\nu c^\dagger_{j\sigma} c_{j+\nu\sigma} + \text{H.c.}) + \sum_j (U n_{j+} n_{j-} - B S^z_j), \tag{2}$$

where $\nu = 1, 2$, $\sigma = \pm 1$, $c^\dagger_{j\sigma}(c_{j\sigma})$ creates (annihilates) an electron of spin σ at site j, $n_{j\sigma} = c^\dagger_{j\sigma} c_{j\sigma}$, $n_j = \sum_\sigma n_{j\sigma}$, and $S^\eta_j = \frac{1}{2} \sum_{\alpha\beta} c^\dagger_{j\alpha} \sigma^\eta_{\alpha\beta} c_{j\beta}$ are the spin-1/2 operators with σ^η being the Pauli matrices. We assume periodic boundary conditions (PBC), i.e., $c^\dagger_{L\sigma} \equiv c^\dagger_{0\sigma}$. The application of the magnetic field increases the uniform magnetization along the field direction z. A spontaneous breaking of the U(1) symmetry of global spin rotation along the z axis is, in this case, prevented by quantum fluctuations. This implies the absence of usual magnetic ordering in the x-y plane: $\langle S^\eta_j \rangle = 0$ with $\eta = x, y$. We will show, however, that nonzero vector and scalar chiralities are simultaneously induced by the field for large enough values of t_2/t_1. The

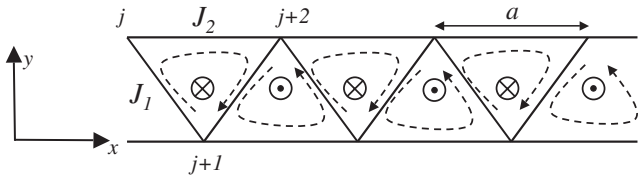

FIG. 1. Zigzag ladder. The arrows indicate the circulation of the spin and the electrical orbital currents that emerge in the ground state for $J_2 \gg J_1$ and $|B| \lesssim |B_{\text{sat}}|$, with B_{sat} the saturation field. The small circles indicate the orientation of the (staggered) magnetic moments generated by the electric currents. (See text for notation.)

vector chiral ordering is a remnant of the classical helical order $\langle S_j^\eta \rangle \neq 0$ that is obtained in the $S \to \infty$ limit [4]. The *scalar* spin chirality results from the spontaneous vector spin chirality and the field-induced magnetization, $\langle \chi_{jkl} \rangle \simeq \langle \mathbf{S}_j \times \mathbf{S}_k \rangle \cdot \langle \mathbf{S}_l \rangle$. This connection between scalar and vector spin chiralities implies a relation between electric and spin currents, i.e., a spin-charge-current effect. This novel effect provides the mechanism to experimentally detect spin currents and/or chiral orders.

For large U/t_ν limit, the low-energy spectrum of H is described by a Heisenberg spin-1/2 Hamiltonian [8],

$$\tilde{H} = \sum_{j,\nu} J_\nu \left(\mathbf{S}_j \cdot \mathbf{S}_{j+\nu} - \frac{1}{4} \right) - B \sum_j S_j^z, \tag{3}$$

because the electrons are localized near the lattice sites j, with vector position $\mathbf{r}_j$. $\tilde{H}$ is obtained by projecting the original H into the low-energy subspace $\mathcal{S}$. This is true in general for any physical quantity, $\mathcal{A}$, whose effective low-energy operator, $\tilde{\mathcal{A}}$, is a function of the spin operators $\mathbf{S}_j$. The expression for $\tilde{\mathcal{A}}$ is obtained by a canonical transformation that follows from standard degenerate perturbation theory. The exchange constants are $J_\nu = 4t_\nu^2/U > 0$.

Two physical quantities are relevant for this work. These are the charge and spin (z component) current densities in a bond $\langle jl \rangle$ ($l = j + \nu$ and $t_{jl} = t_\nu$)

$$\begin{aligned} \mathbf{I}_{jl}^c &= i \sum_\sigma (c_{j\sigma}^\dagger c_{l\sigma} - c_{l\sigma}^\dagger c_{j\sigma}) \frac{e t_{jl}}{\hbar} \hat{\mathbf{r}}_{jl}, \\ \mathbf{I}_{jl}^s &= i \sum_\sigma (c_{j\sigma}^\dagger c_{l\sigma} - c_{l\sigma}^\dagger c_{j\sigma}) \frac{\sigma t_{jl}}{\hbar} \hat{\mathbf{r}}_{jl}, \end{aligned} \tag{4}$$

where $\hat{\mathbf{r}}_{jl} = (\mathbf{r}_l - \mathbf{r}_j)/|\mathbf{r}_l - \mathbf{r}_j|$. Both are Noether currents for the charge and spin conservation laws associated with the corresponding U(1) and SU(2) global symmetries of H. The charge current has a nonzero low-energy effective operator, $\tilde{\mathbf{I}}_{jl}^c$, whenever the site j belongs to a loop that is closed by an odd number of hopping terms [7]. Since the shortest possible loop is a triangle, $\tilde{\mathbf{I}}_{jl}^c$ is $\mathcal{O}(t^n/U^{n-1})$ with n odd and $n \geq 3$. Therefore, the lowest order contribution to the effective charge-current density operator is [7]

$$\tilde{\mathbf{I}}_{jl}^{\,c} = \frac{24e}{\hbar} \hat{\mathbf{r}}_{jl} \sum_{l \neq j,k} \frac{t_{jl} t_{lk} t_{kj}}{U^2} \chi_{jkl}. \tag{5}$$

Equation (5) establishes a direct correspondence between the scalar chiral spin ordering, $\langle \boldsymbol{\chi}_{ijk} \rangle \neq 0$, and the presence of electric orbital currents. In other words, the scalar spin ordering is accompanied by the emergence of orbital currents. The effective spin-current density operator is

$$\tilde{\mathbf{I}}_{jl}^{\,s} = \frac{8t_{jl}^2}{U} \kappa_{jl}^z \frac{\hat{\mathbf{r}}_{jl}}{\hbar}, \quad \text{with} \quad \kappa_{jl}^z = \mathbf{S}_j \times \mathbf{S}_l \cdot \hat{\mathbf{z}}. \tag{6}$$

This simple expression shows that the spin current is directly associated to the vector spin chirality. Since $\mathbf{I}_{jl}^s$ is even under particle-hole transformation ($t_{jl} \to -t_{jl}, \mathbf{S}_j \to -\mathbf{S}_j$), the prefactor on the right-hand side of Eq. (6) can only contain even powers of the hopping amplitudes.

The effective current density operators are necessary to characterize the ground-state correlations when the magnetic field approaches its saturation value $B_{\rm sat}$, and $t_2 \gtrsim t_1$. As we will show below, this ground state exhibits long-range order of spin and charge currents that are roughly proportional to each other when $J_2 \gg J_1$, and $|B| \lesssim |B_{\rm sat}|$. To understand the origin of this instability, it is convenient to write $\tilde{H}$ in terms of new fermionic degrees of freedom f_j by means of the Jordan-Wigner transformation

$$S_j^+ = f_j^\dagger K_j, \qquad S_j^- = K_j f_j, \qquad \bar{n}_j = S_j^z + \tfrac{1}{2}, \tag{7}$$

where $\bar{n}_j = f_j^\dagger f_j$ and $K_j = \prod_{k<j} (1 - 2\bar{n}_k)$ is the nonlocal operator that realizes the change in exchange statistics.

The new expression of $\tilde{H}$ can be written as

$$\begin{aligned} \tilde{H} &= \tilde{H}_1 + \tilde{H}_2 - B \sum_l \bar{n}_l, \\ \tilde{H}_1 &= \frac{J_1}{2} \sum_l (f_l^\dagger f_{l+1} + f_{l+1}^\dagger f_l) + J_1 \sum_l (\bar{n}_l \bar{n}_{l+1} - \bar{n}_l), \\ \tilde{H}_2 &= \frac{-J_2}{2} \sum_l (\kappa_l^z \kappa_{l+1}^z + \kappa_{l+1}^z \kappa_l^z) + J_2 \sum_l (\bar{n}_l \bar{n}_{l+2} - \bar{n}_l), \end{aligned} \tag{8}$$

where $\kappa_l^z \equiv \kappa_{ll+1}^z = i(f_l^\dagger f_{l+1} - f_{l+1}^\dagger f_l)$. We remark that the first term of $\tilde{H}_2$ is an explicit *ferromagnetic* interaction between spin currents on adjacent bonds. However, a state with net nearest-neighbors spin currents, $\langle \kappa_l^z \rangle \neq 0$, can only appear when $J_1 \neq 0$, i.e., for a finite coupling between upper and lower chains (see Fig. 1).

To develop some intuition about the role played by J_1, it is convenient to rewrite $\tilde{H}$ in momentum space

$$\tilde{H} = \sum_k (\epsilon_k - \mu) a_k^\dagger a_k + \frac{1}{2L} \sum_{kqp} v_{pq} a_{q+p}^\dagger a_{k-p}^\dagger a_k a_q, \tag{9}$$

with $a_k^\dagger = \frac{1}{\sqrt{L}} \sum_{j=0}^{L-1} e^{ikj} f_j^\dagger$, $\epsilon_k = J_1 \cos k + J_2 \cos 2k$, $\mu = B + J_1 + J_2$, and $v_{pq} = 2\epsilon_p - 8J_2 \cos(p + 2q)$. The first contribution to v_{pq}, $2\epsilon_p$, contains the density-density interactions of $\tilde{H}_1$ and $\tilde{H}_2$. The second contribution comes from a correlated second-nearest-neighbor hopping that is contained in the first term of $\tilde{H}_2$.

For $J_2 > J_1/4$, the fermion dispersion ϵ_k has two degenerate minima at $k = \pm Q$, with $\cos Q = -J_1/4J_2$, that correspond to opposite values of κ_l^z. The saturation field $B_{\rm sat} = J_1 + J_2 - \epsilon_Q$ ($-B_{\rm sat}$) corresponds to the critical value of the chemical potential at which the fermion density $\rho = \langle \bar{n}_j \rangle$ becomes equal to one (zero). From now on we will assume that the spin system is close to full polarization. Since the physics is independent of the sign of B ($B \to -B$ under time reversal transformation), we will choose the negative sign, $B \gtrsim -B_{\rm sat}$. For the equivalent fermionic problem, this condition is equivalent to the dilute density limit, $\rho \ll 1$ or $\mu \gtrsim \epsilon_Q$.

For $J_1 = 0$, the symmetric and the antisymmetric sectors generated by the fermionic operators $a_k^\dagger \pm a_{k+\pi}^\dagger$ are perfectly decoupled. In this case the spin currents are

quenched since κ_l^z can only connect states on different sectors (it is odd under the transformation $k \to k + \pi$). The situation changes dramatically for $J_1/J_2 \ll 1$. At low energies, we can only have fermions $a_k^\dagger$ near the two degenerate minima: $k \simeq \pm Q$. Since Q is close to $\pi/2$, the fermions $a_{\pm Q}^\dagger$ generate spin currents of nearly maximal amplitude and opposite signs: $\sum_l \kappa_l^z a_k^\dagger |0\rangle = (\sin k) a_k^\dagger |0\rangle$. While the noninteracting part of $\tilde{H}$ favors a ground state in which both minima are equally populated, the second term of v_{pq} leads to a nearest-neighbor attraction between fermions with the same chirality (in the same minimum) and a nearest-neighbor repulsion between fermions with opposite vector chiralities (different minima). This is also expected from the first term of $\tilde{H}_1$ and it implies the possibility of a chiral instability similar to the one originally proposed by Nersesyan and coauthors [1] for XY zigzag spin chains (see also [9]). In fact, the chiral phase was recently found for $J_2 \gg J_1$ and $|B| \simeq B_{\rm sat}$ [4] by using the same mean-field decoupling of the bosonized version of $\tilde{H}$ that was introduced in Ref. [1] for the XY case. A straightforward mean-field approximation to Eq. (9) overestimates the stability of the chiral phase (it gives a wrong density dependence for the energy of the disordered state). Since mean-field approximations to interacting quasi-one-dimensional systems are always subjected to scrutiny, it is decisive to have a numerical confirmation of this phase. By using density-matrix renormalization group (DMRG), Ref. [10] recently found the chiral phase for $J_2 = J_1$, while Ref. [11] reported a phase diagram that confirms the existence of a chiral phase for $J_2 \gg J_1$ and $|B| \simeq B_{\rm sat}$.

We now derive the important physical consequence that allows to measure the vector chiral order parameter. The combination of a field-induced magnetization, $m_z = \langle S_l^z \rangle$, and a net vector spin chirality $\langle \kappa_l^z \rangle \neq 0$ leads to a nonzero mean value of the *scalar spin chirality* ($\boldsymbol{\chi}_l \equiv \chi_{ll+1l+2}$),

$$\boldsymbol{\chi}_l \simeq m_z [\kappa_l^z + \kappa_{l+1}^z - \kappa_{ll+2}^z]. \tag{10}$$

This approximation, valid because of the small m_z fluctuations, shows that scalar and vector chiralities are proportional to each other, with the uniform magnetization m_z being the proportionality constant. The physical meaning becomes clear when we look at Eqs. (1), (5), and (6): the field-induced vector chiral order contains orbital *electric currents* that are proportional to the spin currents

$$\tilde{\mathbf{I}}_{jl}^{\,c} \simeq \frac{6e}{U} m_z \sum_{l \neq j,k} \left[\frac{t_{jl} t_{lk}}{t_{jk}} \tilde{\mathbf{I}}_{jk}^{s} + \frac{t_{jl} t_{jk}}{t_{kl}} \tilde{\mathbf{I}}_{kl}^{s} - \frac{t_{kl} t_{jk}}{t_{jl}} \tilde{\mathbf{I}}_{jl}^{s} \right]. \tag{11}$$

Figure 1 displays the circulation of electrical orbital currents (arrows) expected for the chiral-ordered ground state of the zig-zag chain ($J_2 \gg J_1$ and $|B| \lesssim |B_{\rm sat}|$) according to Eq. (11). Remarkably, the application of a *uniform* magnetic field induces *orbital antiferromagnetism* via the Zeeman coupling to the spin moments. The small circles in Fig. 1 indicate the orientation of the staggered orbital moments that these currents generate.

To test the validity of Eq. (11) we study the ground-state properties of both H and $\tilde{H}$ by means of the DMRG method [12]. We use PBCs [13] to eliminate spurious oscillations in the correlation functions. The incommensurate nature of the ordered ground state makes the numerical calculation quite challenging [14]. In contrast to Ref. [11] we do not include any infinitesimal bias field, and compute chiral-chiral correlators (instead of the order parameter $\langle \kappa_l \rangle$) to establish chiral long-range order. In the case of the Hubbard Hamiltonian H, we solve a chain of $L = 64$ sites for $t_2/t_1 = 1.6$, $U/t_1 = 20$, 24, and 30. B is chosen such that $2m_z = 0.875$. The charge current, $C^c(r) = \langle I_l^c I_{l+r}^c \rangle$, and the spin current, $C^s(r) = \langle I_l^s I_{l+r}^s \rangle$, correlation functions are computed directly in the DMRG ground-state wave function ($\mathbf{I}_{ll+1}^{\gamma} \equiv \mathbf{I}_l^{\gamma}$ with $\gamma = c, s$).

For the Heisenberg model $\tilde{H}$, we study chains of lengths $L = 48$, 64, and 128 sites. The ratio between the exchange constants is determined by the ratio between the hopping amplitudes $J_2/J_1 = t_2^2/t_1^2 = 2.56$, and $2m_z = 0.875$. We compute the vector spin chirality two-point correlation functions: $\bar{C}_{nm}^s(r) = \langle \kappa_{ll+n} \kappa_{l+rl+r+m} \rangle$. Figure 2 shows $\bar{C}_{11}^s(r)$ for different system sizes. The finite-size scaling clearly indicates the presence of long-range vector spin chiral order.

According to Eq. (6), the effective spin-current two-point correlation function is $C^s(r) = [8t_1^2/U]^2 \bar{C}_{11}^s(r)$. At long distances, the effective charge-current correlation function is approximated by using Eq. (10)

$$C^c(r) \simeq \tilde{\alpha} \langle \chi_l \chi_{l+r} \rangle \simeq \tilde{\alpha} m_z^2 [4\bar{C}_{11}^s(r) - 4\bar{C}_{22}^s(r) + \bar{C}_{12}^s(r)], \tag{12}$$

with $\tilde{\alpha} = 2304 t_1^4 t_2^2 / U^4$. Figures 3(a)–3(c) compare the spin-current two-point correlators computed with the Heisenberg ($\tilde{H}$) and the Hubbard (H) models for three different values of $U/t_1 = 20$, 24, and 30.

As expected, the results for the two models show better agreement as U increases. According to Eq. (12), the long-range ordered spin-currents (see Fig. 2) must lead to long-range ordered orbital electric currents. Figures 3(d)–3(f) show a comparison between $C^c(r) = \langle I_l^c I_{l+r}^c \rangle$ computed

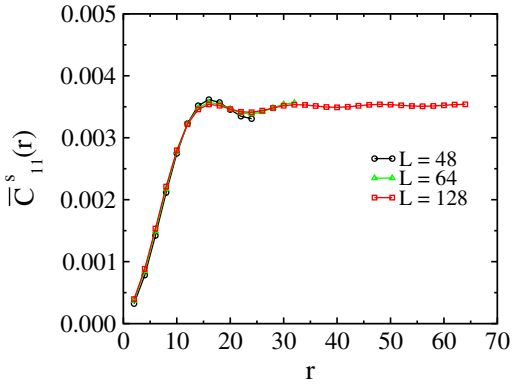

FIG. 2 (color online). Two-point vector spin chirality correlator $\bar{C}_{nm}^s(r)$ for $J_2/J_1 = 2.56$ and $2m_z = 2\langle S_l^z \rangle = 0.875$.

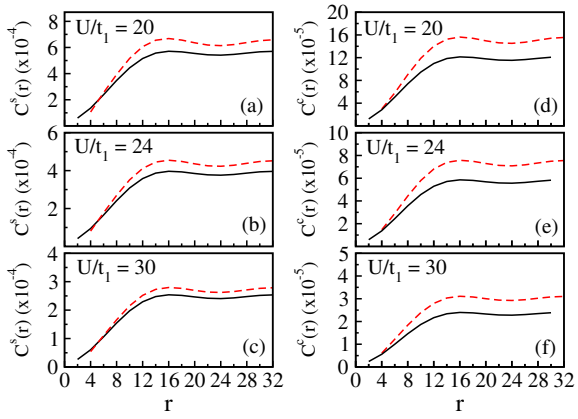

FIG. 3 (color online). (a),(b),(c) Charge-current correlation function $C^c(r)$ and (d),(e),(f) spin-current correlation function $C^s(r)$ in the case of the Hubbard model H (dashed lines) and the Heisenberg model $\tilde{H}$ (solid lines). The results are shown for $L = 64$, $t_2/t_1 = 1.6$ ($J_2/J_1 = 2.56$), $\langle s_i^z \rangle = 0.4375$.

with H for the same three different values of U, and the right-hand side of Eq. (12) computed with the Heisenberg model $\tilde{H}$. The good agreement between both curves confirms that the spin and the electric currents are approximately proportional to each other, with the proportionality constant linear in m_z. In other words, the ordering of spin currents is accompanied by ordering of orbital electric currents for nonzero m_z as follows from Eq. (10).

The resulting staggered configuration of orbital magnetic moments implies that the ground state is a field-induced orbital antiferromagnet. This orbital antiferromagnetism results from the Zeeman coupling to the applied field in contrast to the case of spinless fermion ladder systems in which it is induced by the orbital coupling [15]. We note that the orbital moments are located at the centers of the triangles (see Fig. 1), while the spin moments are obviously located at the corners (lattice sites). The magnitude of the orbital currents are of order 0.01 $et_1/\hbar$ for $U/t_1 = 20$ [see Fig. 3(d)]. The corresponding orbital magnetic moment is a few percent of a Bohr magneton for $t_1 \sim 1$ eV. In contrast to the spin currents $\langle \kappa_i^z \rangle$, these orbital magnetic moments can be measured with experimental techniques such as NS, NMR, or μSR. In particular, the ratio of intensities for the Bragg peaks at wave-vectors $\mathbf{k} = \mathbf{0}$ and $\mathbf{k} = (2\pi/a)\hat{\mathbf{x}}$ ($\hat{\mathbf{x}}$ is a unit vector along the ladder direction; see Fig. 1) will depend on the chiral order parameter because the staggered orbital moments contribute only to the intensity of the second peak while the ferromagnetic spin component contributes to both. On the other hand, the orbital moments will split the NMR and μSR spectra into two different lines. These are simple ways of detecting this exotic spin ordering in real materials. Moreover, the magnitude of the magnetic moment would be much larger if the chiral phase remains stable in the intermediate coupling regime $U \gtrsim t_\nu$.

An externally applied magnetic field can induce an electric current out of a spontaneously generated spin current (or vice versa) because both currents have opposite parity under time reversal and the same parity under spatial inversion. This symmetry consideration has to be complemented by a microscopic mechanism that determines the magnitude of the spin-charge-current conversion. In this work we have derived and quantified such mechanism by exploiting the proportionality between the orbital current and the scalar chirality found in [7]. The combination of Eqs. (5) and (10) allows estimation of the order of magnitude of the orbital electric current, and corresponding orbital magnetic moment, for a given spin current. Since experimental probes (NS, NMR or μSR) can only provide the magnitude of the orbital magnetic moments, the obtained relationships are essential to design experiments oriented to measure the spin currents by detection of the orbital moments. Note that the spin-charge current effect presented here cannot be associated with a magnetoelectric response because the spin current does not couple directly to any electric or magnetic fields.

This work was carried out under the auspices of the NNSA of the U.S. DOE at LANL under Contract No. DE-AC52-06NA25396.

[1] A. A. Nersesyan, A. O. Gogolin, and F. H. L. Essler, Phys. Rev. Lett. **81**, 910 (1998).
[2] J. Villain, Ann. Isr. Phys. Soc. **2**, 565 (1978).
[3] M. Affronte *et al.*, Phys. Rev. B **59**, 6282 (1999).
[4] A. Kolezhuk and T. Vekua, Phys. Rev. B **72**, 094424 (2005).
[5] "hfac" denotes hexafluoro-acetylacetonate and NITR denotes 2-*R*-4, 4, 5, 5-tetramethyl-4,5-dihydro-1H-imidazolyl-1-oxyl 3-oxide, where *R* is isopropyl (iPr), ethyl (Et), methyl (Me), or phenyl (Ph).
[6] S. V. Maleyev *et al.*, J. Phys. Condens. Matter **10**, 951 (1998); S. V. Maleyev, Phys. Rev. Lett. **75**, 4682 (1995).
[7] L. N. Bulaevskii, C. D. Batista, M. Mostovoy, and D. Khomskii, Phys. Rev. B **78**, 024402 (2008).
[8] We are neglecting terms of order t^4/U^3 and higher.
[9] M. Kaburagi, H. Kawamura, and T. Hikihara, J. Phys. Soc. Jpn. **68**, 3185 (1999); T. Hikihara *et al.*, J. Phys. Soc. Jpn. **69**, 259 (2000); Y. Nishiyama, Eur. Phys. J. B **17**, 295 (2000).
[10] I. P. McCulloch *et al.*, Phys. Rev. B **77**, 094404 (2008).
[11] K. Okunishi, J. Phys. Soc. Jpn. **77**, 114004 (2008).
[12] S. R. White, Phys. Rev. Lett. **69**, 2863 (1992); Phys. Rev. B **48**, 10 345 (1993); K. Hallberg, Adv. Phys. **55**, 477 (2006); U. Schollwöck, Rev. Mod. Phys. **77**, 259 (2005); A. F. Albuquerque *et al.*, J. Magn. Magn. Mater. **310**, 1187 (2007).
[13] We keep up to 1200 states and perform up to 20 finite-system sweeps. The weight of the discarded states is $\leq 10^{-11}$.
[14] A. A. Aligia, C. D. Batista, and F. H. L. Essler, Phys. Rev. B **62**, 3259 (2000).
[15] S. T. Carr *et al.*, Phys. Rev. B **71**, 161101 (2005); **73**, 195114 (2006).